ISSN 2176-5480

22nd International Congress of Mechanical Engineering (COBEM 2013)
November 3-7, 2013, Ribeirão Preto, SP, Brazil

RANS MODEL FORMULATIONS FROM LES

Pascoal Escobar
Fernando Soares Alves
Luiz Eduardo Bittencourt Sampaio
Raphael David Aquilino Bacchi
Roney Leon Thompson
Universidade Federal Fluminense - Rua Passo da Pátria 156, São Domingos, Niterói-RJ, Brasil
luizebs@vm.uff.br, rthompson@mec.uff.br

Abstract. *When the Navier-Stokes equations are applied into turbulence, closure equations are necessary in addition to an average approach of the associated variables. These equations relate the Reynolds stress tensor with kinematic tensors. The methodology here presented quantifies the dependence of the Reynolds tensor with kinematic tensors such as the rate-of-strain and the non-persistence-of-strain tensors. The methodology is based on tensor decomposition theorems from the Reynolds stress tensor (anisotropic) obtained from LES are extracted parts in phase and parts out of phase with each kinematic tensor. The proposed RANS basis are then compared with the Reynolds tensor which is obtained by a LES in a backward facing step. Local measurers of the accuracy of each model are employed, becoming possible to quantify their adequacy as a function of the position.The tensor basis used in this study are capable of representing more faithfully the Reynolds stress tensor then the methods used by industry today, and require low computational cost.*

Keywords: *Turbulence modeling; persistence of straining; tensor decomposition;LES*

1. INTRODUCTION

Turbulence is considered one of the most complex phenomena in Physics. Because of that, turbulence modeling is a major active research area in Fluid Mechanics. The most accurate approach is to solve the complete set of the Navier-Stokes equations capturing the very small scales that are necessary for a full description of turbulence, the Direct Numerical Simulation (DNS) method. However, DNS is extremely expensive from the computational point of view, prohibitive for complex geometries. Therefore, this method is restricted for simple cases, and for low Reynolds numbers.

On the other side of the available methods are the so called Reynolds Average Navier-Stokes (RANS). In this case, the Navier-Stokes equations are filtered and only the mean velocity and mean pressure fields are solved. A new term that comes into play is the divergence of the mean velocity fluctuation dyadic, and the Reynolds stress tensor can be defined as $\mathbf{R} = -\overline{\mathbf{u}'\mathbf{u}'}$, where $\overline{(.)}$ indicates the time average operation and a single quote ($'$) denotes the fluctuations with respect to the average. In order to close the set of equations and unknowns, a model for the Reylnods stress tensor connects itself to mean kinematic quantities. RANS models are, by far, the most used approach to solve the turbulence problems faced by industry. The reason is simple, these models are cheap and therefore they fulfill the industrial need for rapid answers. However, the lack of accuracy provided by RANS models defies the use of such approach. In some situations, even the qualitative behavior of the flow is not captured by a traditional RANS model.

An intermediate alternative is the Large Eddy Simulation method (LES). In the LES approach, only the large scales, that carry most of the turbulent energy, are solved; while the small scales, which are costly to solve, are modeled. The advantage of using this approach is that LES is not as expensive as DNS and is much more accurate then RANS. Hence, accurate results for turbulent flows in complex geometry with a relatively high Reynolds number became attainable by using this method.

However, from the industry perspective LES are still costly. The time scale needed for accurate simulations is much higher then the time scale required by the decision making process. This means that RANS models will still be worthy to be used by industry. In this scenario, it would be interesting to improve the accuracy provided by RANS models. One path that can be used in order to achieve this goal is to construct RANS models that are somehow connected to high accurate methods like DNS and LES. The disadvantage of bridging LES-RANS models is that there are two stages of modeling, what means that is a model of a model. The advantage, however, is the possibility of simulating flows in complex geometries with high Reynolds numbers with a high level of accuracy. Therefore, the corresponding RANS model can be generated from complex flows. This advantage cannot be overemphasized, since, in general the results used to feed RANS models come from very simple geometries where the Reynolds stress has a simple structure.

The path adumbrated to build RANS models from LES results consists of two stages. The first one is to extend the usual Boussinesq hypothesis using the projection of the Reynolds stress tensor calculated from the LES approach into mean kinematic tensors subspaces, also calculated from LES, suitably chosen. The second stage is to express the coefficients associated with these projections to mean kinematic scalars, such as the invariants of the mean tensors.

The objective of the present work is to explore the first stage of the bridge LES-RANS. In this connection, the two

ISSN 2176-5480

tensorial entities chosen to describe the Reynolds stress tensor are the symmetric part of the velocity gradient, $\mathbf{D}$, and the non-persistence-of-straining tensor $\mathbf{P}$, discussed by Thompson and Souza Mendes (2005); Thompson (2008)

2. METHODOLOGY

The methodology is the same as the one followed by **?**. The difference lies on the fact that in the present case we use LES results to construct RANS models, while there, the methodology was used to build RANS models from DNS results.

We use two types of decompositions of a generic second order tensor, $\boldsymbol{\mathcal{G}}$, with respect to another symmetric tensor, $\boldsymbol{\mathcal{F}}$ of the following form

$$\boldsymbol{\mathcal{G}} = \boldsymbol{\mathcal{P}}_{\mathcal{G}}^{\mathcal{F}} + \widetilde{\boldsymbol{\mathcal{P}}}_{\mathcal{G}}^{\mathcal{F}}. \tag{1}$$

And we require that this decompositions enjoy the following properties
i) $\boldsymbol{\mathcal{P}}_{\mathcal{G}}^{\mathcal{F}}$ and $\widetilde{\boldsymbol{\mathcal{P}}}_{\mathcal{G}}^{\mathcal{F}}$. are orthogonal;
ii) $\boldsymbol{\mathcal{F}}$ and $\boldsymbol{\mathcal{P}}_{\mathcal{G}}^{\mathcal{F}}$ are coaxial (or commute);
iii) $\boldsymbol{\mathcal{F}}$ and $\widetilde{\boldsymbol{\mathcal{P}}}_{\mathcal{G}}^{\mathcal{F}}$ are orthogonal.

2.1 Tensor decompositions

We use two kinds of decompositions of a symmetric tensor with respect to a second one. The first of these decomposition will be called "proportional-orthogonal decomposition" and decomposes a tensor $\boldsymbol{\mathcal{G}}$ with respect to a target tensor $\boldsymbol{\mathcal{F}}$ as

$$\boldsymbol{\mathcal{G}} = \frac{\mathrm{tr}\left(\boldsymbol{\mathcal{G}}\cdot\boldsymbol{\mathcal{F}}\right)}{\mathrm{tr}\left(\boldsymbol{\mathcal{F}}\cdot\boldsymbol{\mathcal{F}}\right)}\boldsymbol{\mathcal{F}} + \frac{\mathrm{tr}\left(\boldsymbol{\mathcal{F}}\cdot\boldsymbol{\mathcal{F}}\right)\boldsymbol{\mathcal{G}} - \mathrm{tr}\left(\boldsymbol{\mathcal{G}}\cdot\boldsymbol{\mathcal{F}}\right)\boldsymbol{\mathcal{F}}}{\mathrm{tr}\left(\boldsymbol{\mathcal{F}}\cdot\boldsymbol{\mathcal{F}}\right)}, \tag{2}$$

where the first term on the r.h.s. is the part of $\boldsymbol{\mathcal{G}}$ proportional to $\boldsymbol{\mathcal{F}}$ and the second term is orthogonal to $\boldsymbol{\mathcal{F}}$. The second kind, called here "in-phase-out-of-phase decomposition", decomposes a tensor $\boldsymbol{\mathcal{G}}$ with respect to a target tensor $\boldsymbol{\mathcal{F}}$ as

$$\boldsymbol{\mathcal{G}} = \mathbf{1}^{\boldsymbol{\mathcal{F}}\boldsymbol{\mathcal{F}}} : \boldsymbol{\mathcal{G}} + \left(\mathbf{1}^{\delta\delta} - \mathbf{1}^{\boldsymbol{\mathcal{F}}\boldsymbol{\mathcal{F}}}\right) : \boldsymbol{\mathcal{G}}, \tag{3}$$

where $\mathbf{1}^{\boldsymbol{\mathcal{F}}\boldsymbol{\mathcal{F}}}$ and the identity tensor $\mathbf{1}^{\delta\delta}$ are fourth order tensors that are given by

$$\mathbf{1}^{\boldsymbol{\mathcal{F}}\boldsymbol{\mathcal{F}}} = \sum_{i=1}^{3} \mathbf{e}_i^{\mathcal{F}} \otimes \mathbf{e}_i^{\mathcal{F}} \otimes \mathbf{e}_i^{\mathcal{F}} \otimes \mathbf{e}_i^{\mathcal{F}}, \quad \text{and} \quad \mathbf{1}^{\delta\delta} = \mathbf{e}_\mathrm{p} \otimes \mathbf{e}_\mathrm{q} \otimes \mathbf{e}_\mathrm{q} \otimes \mathbf{e}_\mathrm{p}. \tag{4}$$

In Eq. (3), the first term is the in-phase term, which represents the part of tensor $\boldsymbol{\mathcal{G}}$ which is in-phase with tensor $\boldsymbol{\mathcal{F}}$. The second term is the part of $\boldsymbol{\mathcal{G}}$ which is out-of-phase with respect to tensor $\boldsymbol{\mathcal{F}}$. In Eq. (4a) $\mathbf{e}_i^V$ are the unit eigenvectors of tensor $\boldsymbol{\mathcal{F}}$. These two kinds of decomposition were shown by Thompson *et al.* (2010) to be the only ones satisfying the following two properties: the two decomposed parts are respectively coaxial and orthogonal to the target tensor, and these two parts are orthogonal to each other. The mathematical analysis of these two decompositions can be found in Thompson (2008).

2.2 Primitive tensors

The two decompositions presented above can be employed in two different ways: self-correlation and cross-correlation. In this paper we will use the cross-correlation approach. In order to do that, we start with an original tensor like $\boldsymbol{\mathcal{G}}$ above, which we shall try to explain as much as possible by a target tensor – e.g. the tensor $\boldsymbol{\mathcal{F}}$ above. In the present formulation, the deviatoric part of the Reynolds stress tensor is the original tensor that needs to be described in relation to a target tensor. The choice of the latter will be discussed in the next subsection, and will be based on appropriate representations for incompressible turbulent flows. The theory of decomposition can be readily applied to compressible turbulent flows, but for this present investigation we shall concentrate on incompressible flows.

The usual Reynolds decomposition notations will be employed: $\overline{(.)}$ indicates the time average operation and a single quote ($'$) denotes the fluctuations with respect to the average. The Reynolds stress tensor, $\mathbf{R}$, is defined through

$$\mathbf{R} = -\overline{\mathbf{u}'\mathbf{u}'}, \tag{5}$$

where, as usual, the mass density ρ was removed from this term and incorporated into a modified pressure ($p^* = p/\rho$) in the Navier-Stokes equation.

ISSN 2176-5480

The deviatoric part of the Reynolds stress tensor is defined as

$$\mathbf{B} = \mathbf{R} - \frac{1}{3}\mathrm{tr}(\mathbf{R}), \tag{6}$$

where $\mathrm{tr}(.)$ is the trace operator. There are two kinematic tensors that were chosen as "target tensors", to compose the basis of tensors used to explain the Reynolds stress tensor: the symmetric part of the velocity gradient, $\mathbf{D}$ and the non-persistence-of-straining tensor $\mathbf{P}$, defined by

$$\mathbf{P} = [\mathbf{D}, \mathbf{W}^*], \tag{7}$$

where the Lie Bracket $[,]$ is defined as $[\mathbf{A}, \mathbf{B}] \equiv \mathbf{A} \cdot \mathbf{B} - \mathbf{B} \cdot \mathbf{A}$. Tensor $\mathbf{W}^*$ is the relative vorticity tensor, defined as the vorticity measured with respect to the rate of rotation of the eigenvectors of $\mathbf{D}$.

To avoid the computational complexity of calculating the rate of rotation of the eigenvectors, Thompson (2008) showed that the tensor $\mathbf{P}$ can be calculated using the out-of-phase part of the material derivative of tensor $\mathbf{D}$. Since $\mathbf{W}^*$ is a difference between two tensors one that is related to the velocity gradient and the other which is related to the time derivative of the velocity gradient, it seems to be interesting, from a numerical viewpoint, to include a transport equation for $\mathbf{D}$. In this connection, some works in the field of numerical schemes (Yabe *et al.* (1991); Nave *et al.* (2010); Sampaio (2012)) also suggest that there are good reasons for solving a transport equation for gradients of the primitive field. In this context, solving an extra, independent transport equation for gradients (or for $\mathbf{D}$) would not only improve numerical accuracy, but also provide an easier and more precise way to calculate $\mathbf{P}$, to be used in next generation of RANS modeling.

Since $\mathbf{D}$ and $\mathbf{P}$ are orthogonal, we are able to produce 6 levels of representations of the Reynolds stress, depending on the combinations of the decompositions adopted. Besides that, we apply indices of adherence to quantify the ability of the particular model to capture the Reynolds tensor. These indexes (R_I, R_{II}, ...) can be seen as a measure of the theoretical limit intrinsic to each of the models alone, i.e., the best simulation results obtainable in an hypothetical scenario in which the turbulence model is perfect to the point of providing the optimal scalar coefficients.

2.3 Reynolds stress tensor proportional to $\mathbf{D}$

The eddy viscosity (or Boussinesq) hypothesis is based on the assumption that the turbulent shear stress is linearly dependent on the mean velocity gradient, (see Boussinesq (1877); Kolmogorov (1942)), i. e.

$$\mathbf{B} = 2\nu_T \mathbf{D}, \tag{8}$$

where $\mathbf{D}$ is the symmetric part of the mean velocity gradient.

The approach used here is to decompose tensor $\mathbf{B}$ into a tensor which is proportional to $\mathbf{D}$ and a tensor $\mathbf{E}_I$ which is orthogonal to $\mathbf{D}$. Hence,

$$\mathbf{B} = \alpha \mathbf{D} + \mathbf{E}_I, \tag{9}$$

where

$$\alpha = \frac{\mathrm{tr}\,(\mathbf{B} \cdot \mathbf{D})}{\mathrm{tr}\,(\mathbf{D} \cdot \mathbf{D})}. \tag{10}$$

Therefore, α is the best scalar that can be related to the turbulent viscosity defined by Eq.(8). Besides that, tensor E_I can be seen as the error associated with Boussinesq hypothesis.

The scalar quantity α can be scaled with the turbulent kinetic energy k and dissipation rate ϵ to compose a quantity with the dimension of a viscosity, i.e.

$$\alpha = 2C_\mu \frac{k^2}{\epsilon}, \tag{11}$$

where C_μ is a dimensionless scalar.

An important normalized index of the present analysis is a global measure of how important is the term $\alpha\mathbf{D}$ when compared to $\mathbf{B}$, or in other words, how closely Eq.(8) matches DNS or experimental data. This normalized parameter is given by

$$R_I = 1 - \frac{2}{\pi} \cos^{-1} \left(\sqrt{\frac{\mathrm{tr}\,(\alpha^2 \mathbf{D}^2)}{\mathrm{tr}\,(\mathbf{B}^2)}} \right). \tag{12}$$

Parameter R_I is in $[0, 1]$, the limiting cases being $R_I = 0$ when $\alpha\mathbf{D}$ and $\mathbf{B}$ are uncorrelated, and $R_I = 1$ when they are coincident.

ISSN 2176-5480

2.4 Non-linear Reynolds stress model quadratic in the rate-of-strain tensor

A second approach can use the decomposition of the Reynolds stress tensor into a part $\mathbf{\Phi}_B^D$ which is coaxial to the rate-of-strain tensor, and another $\widetilde{\mathbf{\Phi}}_B^D$ which is orthogonal. Mathematically, this is represented by

$$\mathbf{B} = \mathbf{\Phi}_B^D + \widetilde{\mathbf{\Phi}}_B^D = \mathbf{\Phi}_B^D + \mathbf{E}_{II}. \tag{13}$$

The in-phase part, $\mathbf{\Phi}_B^D$, is the part of the Reynolds stress tensor that can be modeled with the rate-of-strain tensor. In other words, if the only information we had about kinematics were tensor $\mathbf{D}$, $\mathbf{\Phi}_B^D$ would be the largest part of the Reynolds stress that could be modeled. Therefore, $\mathbf{\Phi}_B^D$ captures a larger part of $\mathbf{B}$ than $\alpha\mathbf{D}$ in the first decomposition described (see Eq.(9)). The quantity $\mathbf{\Phi}_B^D$ can be written as an isotropic function of $\mathbf{D}$. From the Cayley-Hamilton theorem, it can be shown that $\mathbf{\Phi}_B^D$ is a quadratic function of $\mathbf{D}$,

$$\mathbf{\Phi}_B^D = \alpha_0\mathbf{1} + \alpha_1\mathbf{D} + \alpha_2\mathbf{D}^2. \tag{14}$$

Using the turbulent kinetic energy and the dissipation, we can define the dimensionless coefficients $C_{\mu 0}$, $C_{\mu 1}$, $C_{\mu 2}$ and rewrite Eq. (14) as

$$\mathbf{\Phi}_B^D = C_{\mu 0}k\mathbf{1} + 2C_{\mu 1}\frac{k^2}{\epsilon}\mathbf{D} + C_{\mu 2}\frac{k^3}{\epsilon^2}\mathbf{D}^2. \tag{15}$$

Once the eigenvalues of $\mathbf{\Phi}_B^D$ and $\mathbf{D}$ are known, the three scalar coefficients $(\alpha_0, \alpha_1, \alpha_2)$ are found from solution of the linear system of equations (14) This system has a unique solution. For incompressible flow, taking the trace of Eq.(15) we have

$$3C_{\mu 0}k + C_{\mu 2}\frac{k^3}{\epsilon^2}\mathrm{tr}(\mathbf{D}^2) = 0, \tag{16}$$

which can be used as a check for the values obtained for $C_{\mu 0}$ and $C_{\mu 2}$. We can also construct a global index to measure the weight of $\mathbf{\Phi}_B^D$ on $\mathbf{B}$,

$$R_{II} = 1 - \frac{2}{\pi}\cos^{-1}\left(\sqrt{\frac{\mathrm{tr}\left[\left(\mathbf{\Phi}_{\mathrm{B}}^{\mathrm{D}}\right)^2\right]}{\mathrm{tr}\left(\mathbf{B}^2\right)}}\right). \tag{17}$$

This second index is also a normalized parameter not less then R_I ($0 \leq R_I \leq R_{II} \leq 1$), since it captures the total influence of $\mathbf{D}$ on the Reynolds stress tensor and not only its linear influence. In this sense, the basis presented in subsection 2.3 is a particular case of the above, and therefore a poorer representation of the Reynolds stress tensor.

2.5 Non-linear Reynolds stress model including the persistence of straining tensor

The next step consists of identifying the part of the Reynolds stress tensor that can be explained by the non-persistence-of-straining tensor (see Thompson and Souza Mendes (2005, 2011)), which is orthogonal to $\mathbf{D}$.

$$\mathbf{P} = \mathbf{D}\cdot\mathbf{W}^* - \mathbf{W}^*\cdot\mathbf{D}. \tag{18}$$

In the above equation,

$$\mathbf{W}^* = \mathbf{W} - \mathbf{\Omega}^D, \tag{19}$$

where $\mathbf{W}$ is the skew-symmetric part of the mean velocity gradient (the mean vorticity tensor). The starred $\mathbf{W}$ indicates that this tensor is computed relatively to $\mathbf{\Omega}^D$, the rate of rotation of the eigenvectors of $\mathbf{D}$, defined through

$$\mathbf{\Omega}^D \equiv \dot{\mathbf{e}}_k^D\mathbf{e}_k^D, \tag{20}$$

where $\mathbf{e}_k^D$ are the normalized eigenvectors of $\mathbf{D}$, and $\dot{\mathbf{e}}_k^D$ are their time derivatives.

The three term basis representation ($\mathbf{D}$, $\mathbf{D^2}$ and $\mathbf{P}$) was previously used by Rumsey *et al.* (2000) in a non-linear turbulence model and by Mompean *et al.* (2003) for a viscoelastic algebraic extra-stress constitutive equation.

Obtaining tensor $\mathbf{P}$ can be a difficult task since, from Eq.(20), the rate of change of the eigenvectors of $\mathbf{D}$ have to be calculated. In Thompson *et al.* (2010) it is shown how the decomposition in the in-phase and out-of-phase parts of a

ISSN 2176-5480

tensor makes the evaluation the persistence of straining tensor $\mathbf{P}$ easier and computationally cheaper, without having to evaluate the rate of rotation of the eigenvectors of $\mathbf{D}$.

Once $\mathbf{P}$ is known, and using the fact that this tensor is orthogonal to $\mathbf{D}$, we can search for the part of $\widetilde{\mathbf{\Phi}}_B^D$ that is proportional to $\mathbf{P}$. Thus, the decomposition stated by Eq.(13) can be written in another form as

$$\mathbf{B} = \mathbf{\Phi}_B^D + \beta\,\mathbf{P} + \mathbf{E}_{III}, \tag{21}$$

where $\mathbf{E}_{III} = \widetilde{\mathbf{\Phi}}_B^D - \beta\,\mathbf{P}$ is mutually orthogonal to $\mathbf{D}$ and $\mathbf{P}$. The determination of β follows the same lines of Eq.(10), i. e.

$$\beta = \frac{\mathrm{tr}\left[\widetilde{\mathbf{\Phi}}_{\mathrm{B}}^{\mathrm{D}} \cdot \mathbf{P}\right]}{\mathrm{tr}\left[\mathbf{P}^2\right]}. \tag{22}$$

Having found β we are now able to define a third index as

$$R_{III} = 1 - \frac{2}{\pi}\cos^{-1}\left(\sqrt{\frac{\mathrm{tr}\left[\left(\mathbf{\Phi}_{\mathrm{B}}^{\mathrm{D}} + \beta\,\mathbf{P}\right)^2\right]}{\mathrm{tr}\,\mathbf{B}^2}}\right), \tag{23}$$

enjoying the property $0 \leq R_I \leq R_{II} \leq R_{III} \leq 1$.

Similarly to what was done in the previous section, we can construct a dimensionless coefficient, C_β, based on the parameter β. Since tensor $\mathbf{P}$ has the same dimension as $\mathbf{D}^2$,

$$\beta = C_\beta \frac{k^3}{\epsilon^2}. \tag{24}$$

2.6 A Reynolds stress model which is linear on the rate of strain and on the persistence of straining tensor

An intermediate level of approximation is achieved by writing the anisotropic Reynolds stress tensor as a linear function of $\mathbf{D}$ and $\mathbf{P}$ as

$$\mathbf{B} = \alpha\mathbf{D} + \beta\,\mathbf{P} + \mathbf{E}_{IV}, \tag{25}$$

where $\mathbf{E}_{IV}$ is the error associated to this fourth hypothesis model. In this case, the model resembles the simplified form proposed by Shih *et al.* (1995). The difference lies on the fact that the tensor $\mathbf{P}$ in the model proposed by Shih *et al.* (1995) uses the vorticity tensor in the place of the relative-vorticity tensor in Eq. (18). Here, we can notice that from the concept of the decompositions adopted, the coefficients α and β are the same of those calculated from models M_I and M_{II}. The index R_{IV} can also be calculated with the analogous expression given by

$$R_{IV} = 1 - \frac{2}{\pi}\cos^{-1}\left(\sqrt{\frac{\mathrm{tr}\left[\left(\alpha\mathbf{D} + \beta\,\mathbf{P}\right)^2\right]}{\mathrm{tr}\,\mathbf{B}^2}}\right). \tag{26}$$

2.7 A Reynolds stress model linear on the mean strain rate and non-linear on the persistence of straining tensor

An approach which was not explored previously in the literature is a model which is proportional to the mean rate of strain and in-phase with the persistence-of-straining tensor.

$$\mathbf{B} = \alpha\mathbf{D} + \mathbf{\Phi}_B^P + \mathbf{E}_V, \tag{27}$$

where $\mathbf{E}_V$ is the error associated to this fifth level of the non-linear model. Analogously to what was done with tensor $\mathbf{\Phi}_B^D$, the quantity $\mathbf{\Phi}_B^P$ can be written as

$$\mathbf{\Phi}_B^P = \beta_0\mathbf{1} + \beta_1\mathbf{P} + \beta_2\mathbf{P}^2. \tag{28}$$

Using dimensionless coefficients, we can write

$$\mathbf{\Phi}_B^P = C_{\beta 0}k\mathbf{1} + C_{\beta 1}\frac{k^3}{\epsilon^2}\mathbf{P} + C_{\beta 2}\frac{k^5}{\epsilon^4}\mathbf{P}^2. \tag{29}$$

ISSN 2176-5480

Here, we can notice that from the concept of the decompositions adopted, the coefficients α and β are the same of those calculated from models M_I and M_{II}. Analogously, the index R_V can also be calculated with the expression:

$$R_V = 1 - \frac{2}{\pi}\cos^{-1}\left(\sqrt{\frac{\mathrm{tr}\left[\left(\alpha\mathbf{D} + \mathbf{\Phi}_{\mathrm{B}}^{\mathrm{P}}\right)^2\right]}{\mathrm{tr}\,\mathbf{B}^2}}\right). \tag{30}$$

2.8 A Reynolds stress model in-phase with the mean strain rate and in-phase with the persistence of straining tensor

The last approach presented here is the most completed one and has not been explored in the literature so far. It is a model that is in-phase with the mean rate of strain and in-phase with the persistence-of-straining tensor:

$$\mathbf{B} = \mathbf{\Phi}_B^D + \mathbf{\Phi}_B^P + \mathbf{E}_{VI}, \tag{31}$$

where $\mathbf{E}_{VI}$ is the error associated to this fifth level of representation. The index R_{VI} is given by

$$R_{VI} = 1 - \frac{2}{\pi}\cos^{-1}\left(\sqrt{\frac{\mathrm{tr}\left[\left(\mathbf{\Phi}_{\mathrm{B}}^{\mathrm{D}} + \mathbf{\Phi}_{\mathrm{B}}^{\mathrm{P}}\right)^2\right]}{\mathrm{tr}\,\mathbf{B}^2}}\right). \tag{32}$$

3. RESULTS

For the sake of clarity and for easier referencing in this section, we provide below a summary of the six models presented above:

$$M_I:\ \mathbf{B}_I = \alpha\mathbf{D} \tag{33}$$

$$M_{II}:\ \mathbf{B}_{II} = \alpha_0\mathbf{I} + \alpha_D\mathbf{D} + \alpha_{D2}\mathbf{D}^2 \tag{34}$$

$$M_{III}:\ \mathbf{B}_{III} = \alpha_0\mathbf{I} + \alpha_D\mathbf{D} + \alpha_{D2}\mathbf{D}^2 + \beta\mathbf{P} \tag{35}$$

$$M_{IV}:\ \mathbf{B}_{IV} = \alpha\mathbf{D} + \beta\mathbf{P} \tag{36}$$

$$M_V:\ \mathbf{B}_V = \beta_0\mathbf{I} + \alpha\mathbf{D} + \beta_P\mathbf{P} + \beta_{P2}\mathbf{P}^2 \tag{37}$$

$$M_{VI}:\ \mathbf{B}_{VI} = (\alpha_0 + \beta_0)\,\mathbf{I} + \alpha_D\mathbf{D} + \alpha_{D2}\mathbf{D}^2 + \beta_P\mathbf{P} + \beta_{P2}\mathbf{P}^2 \tag{38}$$

and the indexes, $R_i, i \in \{I, II, III, IV, V, VI\}$ that measure the quality of the approximations are given by

$$R_i = 1 - \frac{2}{\pi}\cos^{-1}\sqrt{\frac{\mathrm{tr}\,\mathbf{B}_{\mathrm{i}}^2}{\mathrm{tr}\,\mathbf{B}^2}}. \tag{39}$$

In Eq. (39), $\mathbf{B}_i$ are the deviatoric Reynolds stress tensor projected in the i-basis, while $\mathbf{B}$ is the deviatoric Reynolds stress tensor that comes from the DNS data. The indices given by Eq. (39) were shown Thompson (2008) to provide a normalized quantity with the following property

$$\phi_U^V + \widetilde{\phi}_U^V = 1 - \frac{2}{\pi}\cos^{-1}\sqrt{\frac{\mathrm{tr}\left(\mathbf{\Phi}_{\mathrm{U}}^{\mathrm{V}}\right)^2}{\mathrm{tr}\,\boldsymbol{\mathcal{G}}^2}} + 1 - \frac{2}{\pi}\cos^{-1}\sqrt{\frac{\mathrm{tr}\left(\widetilde{\mathbf{\Phi}}_{\mathrm{U}}^{\mathrm{V}}\right)^2}{\mathrm{tr}\,\boldsymbol{\mathcal{G}}^2}} = 1 \tag{40}$$

The quantities R_i are local. It is straightforward to infer that, at any point of the domain, the following inequalities hold:

$$0 \le R_I \le R_{II} \le R_{III} \le R_{VI} \le 1 \tag{41}$$

$$0 \le R_I \le R_{IV} \le R_{III} \le R_{VI} \le 1 \tag{42}$$

$$0 \le R_I \le R_{IV} \le R_V \le R_{VI} \le 1 \tag{43}$$

From the inequalities above, we can establish the different complexity levels of approximation. One important issue is to address the differences between models of the same level of complexity such as the pair M_{II} and M_{IV} and the pair M_{III} and M_V.

ISSN 2176-5480

4. NUMERICAL FORMULATION

4.1 Geometry: Backward facing step

The backward facing step is a classical benchmark test case, and has been extensively used in the literature to validate turbulence models. Here we use the same geometry as Le *et al.* (1997), with a 1.2 expansion ratio ($ER = L_y - h/L_y$, with $L_y = 6h$), shown in Fig. 1. The other dimensions are $L_x = 23h$, $L_z = 4h$, and $L_i = 3h$, where h is the step height, L_i is the inlet length, before the step, and L_x, L_y, L_z are the total length, height and span, respectively.

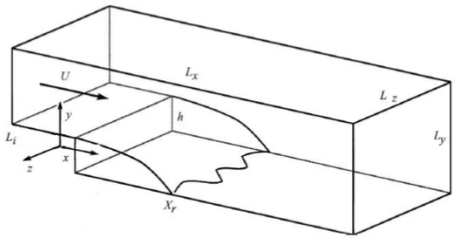

Figure 1. Backward facing step geometry

The inlet boundary conditions are: imposed velocity, according to a profile obtained with DNS ((Le *et al.*, 1997)) at $x = -3h$ from the step. The step height based Reynolds number was $Re = U_0 h/\nu = 5100$, where U_0 is the maximum velocity, and ν is the kinematic viscosity. Zero gradient in normal direction is also imposed on the pressure field. For simplicity, turbulence is not set there, in a hope that at least some part of the spectrum would have developed before reaching the step, and that the abrupt geometry will provide most of the turbulence downstream.

The outlet is set as an outflow, with fixed pressure (zero) and null normal gradient for the velocity and turbulence variables.

The bottom surfaces are set as walls, while the top, as an impenetrable, no-stress plane. The lateral planes are set as periodic.

4.2 Discretization

To solve the governing equations in a computer, a discretization process is needed to project the complete and continuous function space and operators into a vectorial space, resulting in a linear system to be solved.

The mass, momentum, and turbulence equations were discretized using the Finite Volume Method (FVM) implemented in OpenFOAM (OpenFOAM version 2.1.1). The field values are stored at the control volume centroids. Whenever fluxes or other face quantities are needed, the centroid values are interpolated to the faces centroids, using the most appropriate scheme. Here, a linear interpolation is used for the velocity field, corresponding to the classical central differences scheme of Finite Difference Method (FDM). This avoids extra dissipation which would otherwise affect the turbulence spectrum, and it is the recommended scheme when a physical modeling approach is chosen over an implicit LES. On the other hand, for variables like the subgrid turbulent kinetic energy, which cannot assume negative values and should be bounded, a Total Variation Diminishing (TVD) scheme based on Minmod limiter is employed. This guarantees a bounded behavior when high frequency oscillations are eminent, yet an accurate discretization for smoother modes.

The discretization of these equations generates three sets of linear systems, corresponding to the mass, momentum, and subgrid turbulence equations, which are solved separately, in a segregated approach. During a time step of the transient evolution, the momentum is solved first, then the pressure is found to correct the mass conservation, and lastly the subgrid energy is solved to update the find the temperature, based on the velocity found in the other two steps. Numerical experiments suggested that the temperature-velocity coupling inside a single time step is far less important than the velocity-pressure coupling. Therefore, an inner loop coupling is performed only for the velocity and pressure fields, using the PISO methodology (Issa, 1986).

An hexahedral mesh consisting of $300 \times 160 \times 32$ subdivisions in the streamwise (x), vertical (y) and spanwise (z) directions respectively was employed. In the x-direction, 40 subdivisions out of the total (300) were placed before the step, with a small concentration towards the step. Also, in the y-direction a non-uniform distribution of subdivisions was employed, concentrating control volumes close to the wall and in the step level. After simulation was ran and the mean wall shear stress was obtained, it was possible to evaluate the near wall normal spacing in wall units, $\Delta y^+ = \Delta y/\delta$. The wall characteristic length is given by $\delta = \nu/u_* = \nu/\sqrt{\tau_w/\rho}$, where τ_w is the local mean wall shear stress. The resulting near wall mesh spacing in wall units were $\Delta y^+ = 0.56$ in average, and $\Delta y^+ = 7.57$ in the worst case, indicating that a suitable resolution was obtained to tackle turbulence with LES.

ISSN 2176-5480

4.3 LES Model

The Navier-Stokes equation and continuity are implicitly filtered in space, taking advantage of the Finite Volume Methods integral over each control volume. The resulting equation presents an additional term representing the subgrid (filtered) scales and its interaction with the resolved scales, and needs modeling as it cannot be closed. This term is modeled according to the Boussinesq hypothesis, in the framework of a functional model, where the dissipative role it plays in the energy cascade is more important than the exact capturing of the subgrid stress tensor structure.

The subgrid stress tensor, or more precisely, its deviatoric part, is thus assumed tied to the symmetric part of the resolved velocity gradient, by means of a "subgrid" viscosity, which is the very essence of all the modeling involved.

To provide the local value of this viscosity, two characteristics quantities are generally needed. Among the various modeling options, we choose the one equation subgrid model of Horiuti (Yoshizawa and Horiuti, 1985), in which the two characteristic values are the subgrid kinetic energy (k_{SGS}), given by its own additional transport equation, and a length scale, given by the cubic root of the control volume volume. The constant parameters of the model were dynamically adjusted, locally and for each time step, following the Germano methodology (Germano *et al.*, 1991; Ghosal *et al.*, 1995).

5. RESULTS

5.1 Validation of LES results

In order to validate our LES results, before we use them to construct a RANS formulation, we compare some quantities with the DNS results obtained in the literature. Here we report some of them, taken after 6h, 10h, 15h, and 19h so that the reader can analyze how was the evolution of the results accuracy with respect to CPU time.

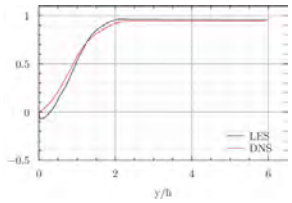

Figure 2. Velocity at a certain position after 6 hours of CPU time.

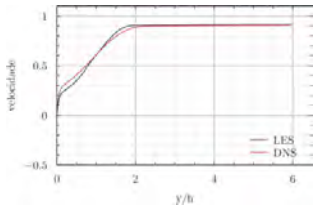

Figure 3. Velocity at a certain position after 10 hours of CPU time.

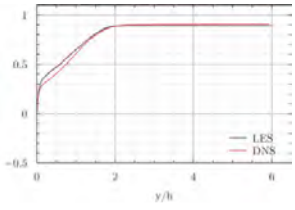

Figure 4. Velocity at a certain position after 15 hours of CPU time.

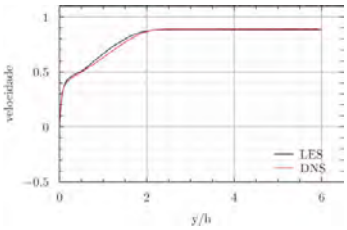

Figure 5. Velocity at a certain position after 19 hours of CPU time.

ISSN 2176-5480

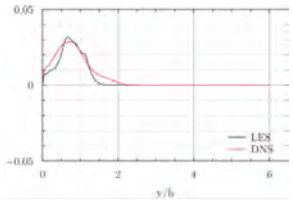

Figure 6. Reynolds stress component R_{xx} at a certain position after 6 hours of CPU time.

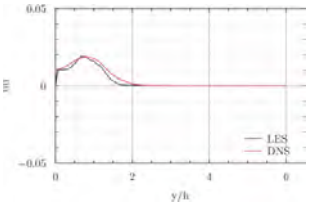

Figure 7. Reynolds stress component R_{xx} at a certain position after 10 hours of CPU time.

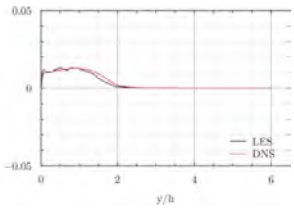

Figure 8. Reynolds stress component R_{xx} at a certain position after 15 hours of CPU time.

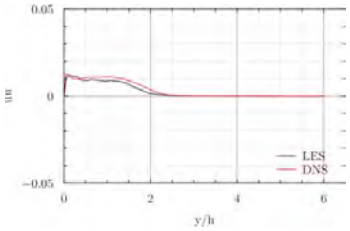

Figure 9. Reynolds stress component R_{xx} at a certain position after 19 hours of CPU time.

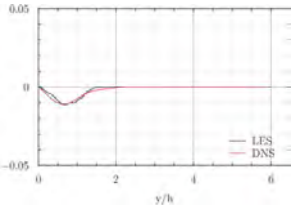

Figure 10. Reynolds stress component R_{xy} at a certain position after 6 hours of CPU time.

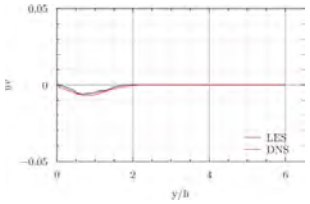

Figure 11. Reynolds stress component R_{xy} at a certain position after 10 hours of CPU time.

5.2 Indices of model performance

A global measurer of the model performance is given by the indices shown in the methodology that give the norm of the Reynolds stress predicted by the model, normalized by the norm of the Reynolds stress predicted by the LES calculations. Below, we show the results for all these indices, from R_I to R_{VI}.

ISSN 2176-5480

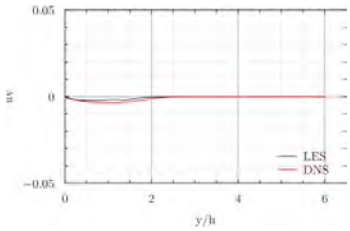

Figure 12. Reynolds stress component R_{xy} at a certain position after 15 hours of CPU time.

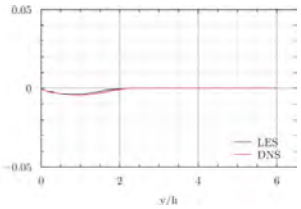

Figure 13. Reynolds stress component R_{xy} at a certain position after 19 hours of CPU time.

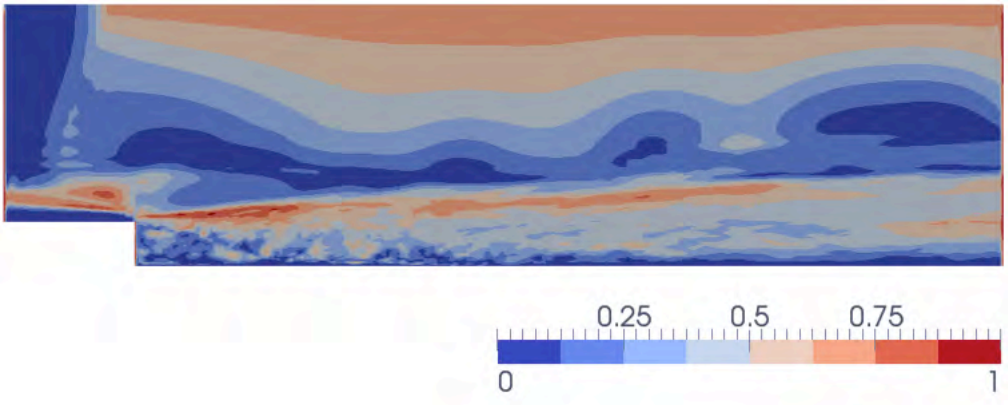

Figure 14. Index R_I, related to model M_I.

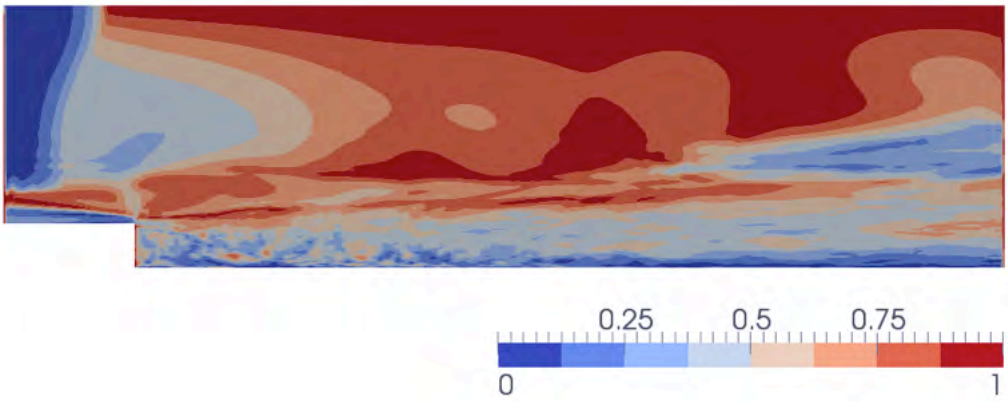

Figure 15. Index R_{II}, related to model M_{II}.

6. CONCLUSIONS

The methodology was successfully employed with the indices corresponding to more complete models providing a better representation of the Reynolds stress tensor that was originated by a LES approach. The Boussinesq hypothesis was shown to be a very poor representation for the Reynolds stress tensor. At the inlet, all the models had a poor performance. This fact was due to a vanishing Reynolds stress tensor at the entrance. Therefore, no model could give a good representation. A possible path to circumvent this problem is to model the full tensor, including the term with the molecular viscosity.The next step is to propose functions for the coefficients.

ISSN 2176-5480

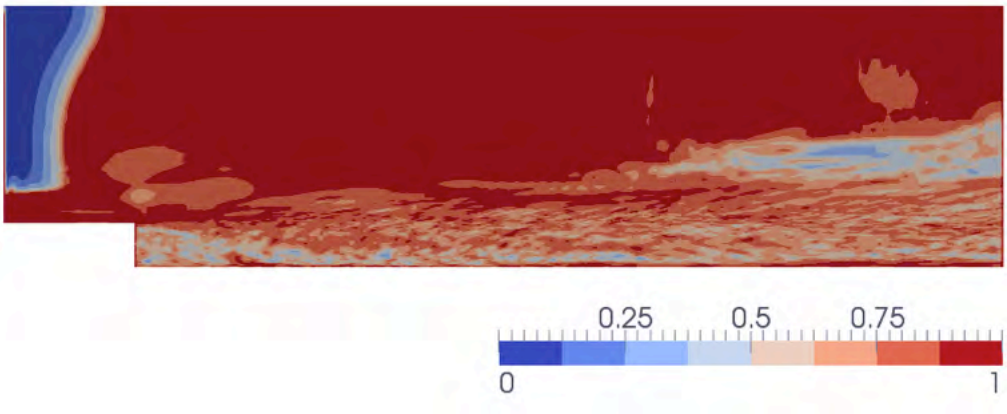

Figure 16. Index R_{III}, related to model M_{III}.

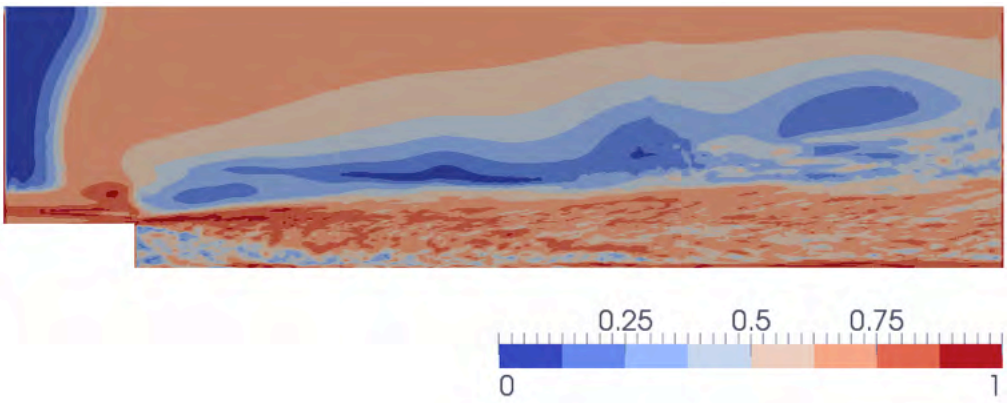

Figure 17. Index R_{IV}, related to model M_{IV}.

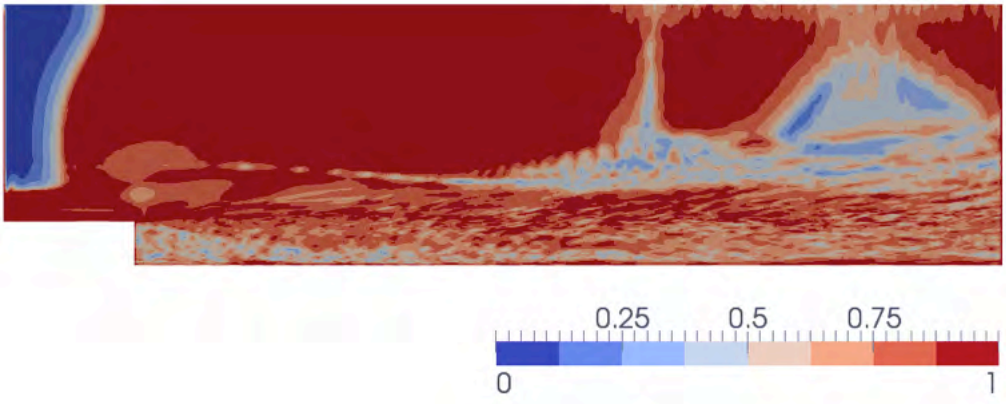

Figure 18. Index R_V, related to model M_V.

7. REFERENCES

Boussinesq, M., 1877. "Essai sur la theorie des eaux courantes". *Mem. pres. Acad. Sci., 3rd edn, Imprimerie Nationale, Paris*, Vol. XXIII, p. 46.

Germano, M., Piomelli, U., Moin, P. and Cabot, W., 1991. "A dynamic subgrid-scale eddy viscosity model". *Physics of Fluids A: Fluid Dynamics*, Vol. 3, p. 1760.

Ghosal, S., Lund, T., Moin, P. and Akselvoll, K., 1995. "A dynamic localization model for large-eddy simulation of turbulent flows". *Journal of Fluid Mechanics*, Vol. 286, pp. 229–255.

Issa, R.I., 1986. "Solution of the implicitly discretised fluid flow equations by operator-splitting". *Journal of Computational Physics*, Vol. 62, pp. 40–65. doi:10.1016/0021-9991(86)90099-9.

Kolmogorov, A.N., 1942. "Equations of turbulent motion of an incompressible fluid". *Izvest. Acad. of Sci., SSSR; Physics*, Vol. 6, pp. 56–58.

ISSN 2176-5480

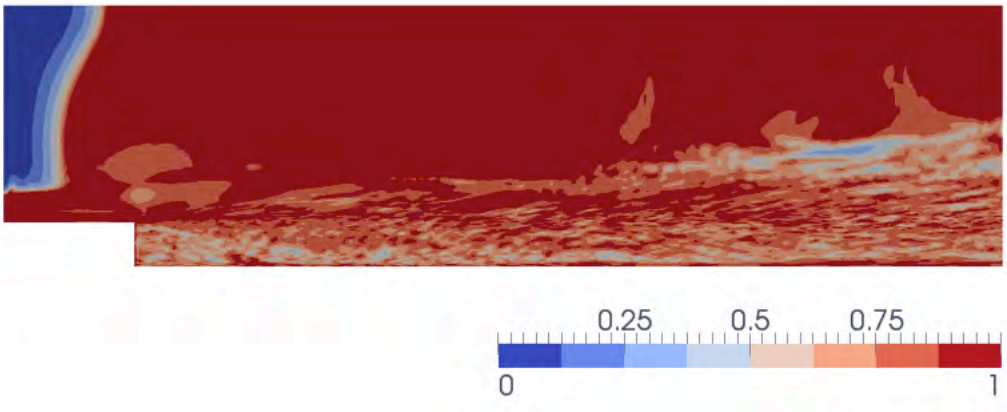

Figure 19. Index R_{VI}, related to model M_{VI}.

Le, H., Moin, P. and Kim, J., 1997. "Direct numerical simulation of turbulent flow over a backward-facing step". *Journal of Fluid Mechanics*, Vol. 330, pp. 349–374.

Mompean, G., Thompson, R.L. and Souza Mendes, P.R., 2003. "A general transformation procedure for differential viscoelastic models". *J. Non-Newtonian Fluid Mech.*, Vol. 111, pp. 151–174.

Nave, J.C., Rosales, R. and Seibold, B., 2010. "A gradient-augmented level set method with an optimally local, coherent advection scheme". *Journal of Computational Physics*, Vol. 229, No. 10, pp. 3802–3827. ISSN 00219991.

OpenFOAM version 2.1.1, 2013. "Userguide and programmers guide". www.openfoam.org.

Rumsey, C.L., Gatski, T.B. and Morrison, J.H., 2000. "Turbulence model predictions of strongly curved flow in a U-duct". *AIAA Journal*, Vol. 38, No. 8, pp. 1394–1402.

Sampaio, L.E.B., 2012. "A transport-physics-accurate convection discretization based on first order upwind and the need for a new error assessment strategy". *Computers & Fluids*, Vol. 67, No. 0, pp. 87 – 103. ISSN 0045-7930. doi:10.1016/j.compfluid.2012.07.013. URL `http://www.sciencedirect.com/science/article/pii/S0045793012002812`.

Shih, T., Zhu, J. and Lumley, J.L., 1995. "A new Reynolds stress algebraic equation model". *Comp. Meth. Appl. Mech. Engng.*, Vol. 125, pp. 287–302.

Thompson, R.L., 2008. "Some perspectives on the dynamic history of a material element". *Int. J. Engng. Sci*, Vol. 46, pp. 524–549.

Thompson, R.L., Mompean, G. and Thais, L., 2010. "A methodology to quantify the non-linearity of the Reynolds stress tensor." *J. Turb.*, Vol. 11, pp. 1–27.

Thompson, R.L. and Souza Mendes, P.R., 2005. "Persistence of straining and flow classification". *Int. J. Engng. Sci*, Vol. 43, No. 1-2, pp. 79–105.

Thompson, R.L. and Souza Mendes, P.R., 2011. "Constitutive equations for non-newtonian fluids based on the persistence-of-straining tensor". *Mecc*, Vol. 46, pp. 1035–1045.

Yabe, T., Aoki, T., Sakaguchi, G., Wang, P. and Ishikawa, T., 1991. "The compact CIP (cubic-interpolated pseudo-particle) method as a general hyperbolic solver". *Computers & Fluids*, Vol. 19, No. 3-4, pp. 421–431. ISSN 00457930. doi: 10.1016/0045-7930(91)90067-R.

Yoshizawa, A. and Horiuti, K., 1985. "A statistically-derived subgrid-scale kinetic energy model for the large-eddy simulation of turbulent flows". *Journal of the Physical Society of Japan*, Vol. 54, No. 8, pp. 2834–9.

8. RESPONSIBILITY NOTICE

The authors are the only responsible for the printed material included in this paper.